A Journal of the Gesellschaft Deutscher Chemiker
Angewandte Chemie
GDCh
International Edition
www.angewandte.org

Accepted Article

Title: Schottky barrier-induced surface electric field boosts universal reduction of NOx- in water to ammonia

Authors: Peng Gao, Zhong-Hua Xue, Shi-Nan Zhang, Dong Xu, Guang-Yao Zhai, Qi-Yuan Li, Jie-Sheng Chen, and Xin-Hao Li

To be cited as: *Angew. Chem. Int. Ed.* 10.1002/anie.202107858

Link to VoR: https://doi.org/10.1002/anie.202107858

WILEY-VCH

10.1002/anie.202107858

WILEY-VCH

COMMUNICATION

Schottky barrier-induced surface electric field boosts universal reduction of NO_x^- in water to ammonia

Peng Gao,[a] Zhong-Hua Xue,[a, b] Shi-Nan Zhang,[a] Dong Xu,[a] Guang-Yao Zhai,[a] Qi-Yuan Li,[a] Jie-Sheng Chen[a] and Xin-Hao Li*[a]

[a] P. Gao, Z. H. Xue, S. N. Zhang, D. Xu, G. Y. Zhai, Q. Y. Li, Prof. J. S. Chen, Prof. X. H. Li
School of Chemistry and Chemical Engineering
Shanghai Jiao Tong University
Shanghai 200240 (P. R. China)
*E-mail: xinhaoli@sjtu.edu.cn

[b] Z. H. Xue
Department of Applied Chemistry
Anhui Agricultural University
Hefei 230036 (P. R. China)

Abstract: NO_x^- reduction acts a pivotal part in sustaining globally balanced nitrogen cycle and restoring ecological environment, ammonia (NH_3) is an excellent energy carrier and the most valuable product among all the products of NO_x^- reduction reaction, the selectivity of which is far from satisfaction due to the intrinsic complexity of multiple-electron NO_x^--to-NH_3 process. Here, we utilize the Schottky barrier-induced surface electric field, by the construction of high density of electron-deficient Ni nanoparticles inside nitrogen-rich carbons, to facilitate the enrichment and fixation of all NO_x^- anions on the electrode surface, including NO_3^- and NO_2^-, and thus ensure the final selectivity to NH_3. Both theoretical and experimental results demonstrate that NO_x^- anions were continuously captured by the electrode with largely enhanced surface electric field, providing excellent Faradaic efficiency of 99 % from both electrocatalytic NO_3^- and NO_2^- reduction. Remarkably, the NH_3 yield rate could reach the maximum of 25.1 mg h^{-1} cm^{-2} in electrocatalytic NO_2^- reduction reaction, outperforming the maximum in the literature by a factor of 6.3 in neutral solution. With the universality of our electrocatalyst, all sorts of available electrolytes containing NO_x^- pollutants, including seawater or waste water, could be directly used for ammonia production in potential through sustainable electrochemical technology.

Over the past century, a massive amount of NO_x was discharged into the ecosystems worldwide owing to the combustion of nitrogen-containing fuels and drainage of N-rich industrial and agricultural sewage, resulting in the pollution of NO_x^- species in water, including NO_3^- and NO_2^-, with adverse cascade effects on the environment and human health.[1] Therefore, the management of soluble NO_x^- anions is essential to address these severe issues and maintain a globally balanced nitrogen cycle.[2] Traditional methods for NO_x^- degradation mainly include biological nitrogen remediation, reverse osmosis and ion exchange, which still suffer from the disadvantages of inert kinetics, harsh conditions, complicated processes and high cost.[3]

Selective reduction of NO_x^- by using reusable heterogeneous catalysts and sustainable electricity to generate harmless nitrogen gas or useful ammonia-regarded as an energy carrier promise the blue print of NO_x^- reduction without the involvement of reductants and other additives.[4] Recent successes in selective reduction of NO_3^- on noble metal nanocatalysts could achieve high Faradaic efficiencies for ammonia production in various acid or basic solutions.[5] Considering the requirements of zero emission for NO_x^- reduction, further boosting the selectivity to ammonia in neutral catalytic system without adding acid or base still remains challenging. From the aspect of selectivity, the reduction of toxic NO_2^- is more urgent to be removed from water.[6] The selectivity of ammonia in both NO_3^- and NO_2^- reduction reactions on reported transition metal-based nanocatalysts was still far from satisfaction. As a result, it is of great practical significance to develop powerful, cheap and durable nanocatalysts for universal reduction of soluble NO_x^- anions, including NO_3^- and NO_2^-, with high Faradaic efficiencies and high yields of ammonia especially in neutral solution.

Herein, we present the concept-new application of Schottky barrier-induced surface electric field in a dyadic electrocatalyst to universally boost the capture and electrocatalytic activation of all NO_x^- in water for selective production of ammonia. We developed a sulfur-diffusion method to successfully integrate record-high density of metallic Ni nanoparticles (35 wt. %) inside nitrogen-rich (10.2 at. %) carbon support (Ni/NC-sd) without consuming their nitrogen contents, as confronted by conventional carbothermal methods with a tradeoff between metal and nitrogen dopant contents (Ni/NC-ct).[7] The well-maintained rectifying contact of nickel/nitrogen-rich carbon interface with electron-deficient Ni and electron-rich carbon afford us the ability to elevate the electric field density of the catalyst surface by merging more Ni/NC heterojunctions together.[8] The experimental and theoretical results demonstrate the key role of more pronounced surface electric field in Ni/NC-sd in capturing and enriching all NO_x^- anions for highly selective production of ammonia, providing the state-of-the-art Faradaic efficiencies and yields of ammonia from the reduction of NO_3^- and NO_2^- for real-life uses at wide concentration range even in electrolyte-free water.

In order to integrate more Ni nanoparticles in/on carbon support without scarifying the nitrogen concentration, we developed a sulfur-diffusion method (Figure 1a) to transform Ni plates to tiny Ni nanoparticles inside the as-formed nitrogen-rich carbons (Figure 1b) from thermal condensation of dicyandiamide as presented in Figure S1. Such a sulfur-diffusion path uses the low-temperature reaction between Ni metal plate and ammonium sulfate to give Ni_3S_2 followed by high-temperature decomposition of Ni_3S_2 back to metallic Ni (Figure 1c and Figure S2) with all the S species released to N_2 gas flow (Figure S3).[9] The Ni contents of Ni_x/NC-sd samples (Figure 1d and Table S1) could be gradually increased by adding more ammonium sulfate in the precursor without consuming the reductive nitrogen dopants (Figure S4 and Table S1) and changing the mean sizes of Ni nanoparticles (Figure S5) and surface areas of the hybrids (Figure S6). Indeed, the as-obtained Ni_x/NC-sd samples exhibit constant nitrogen contents of 10.2 at. % (Figure 1d), which is 3.3 times

10.1002/anie.202107858

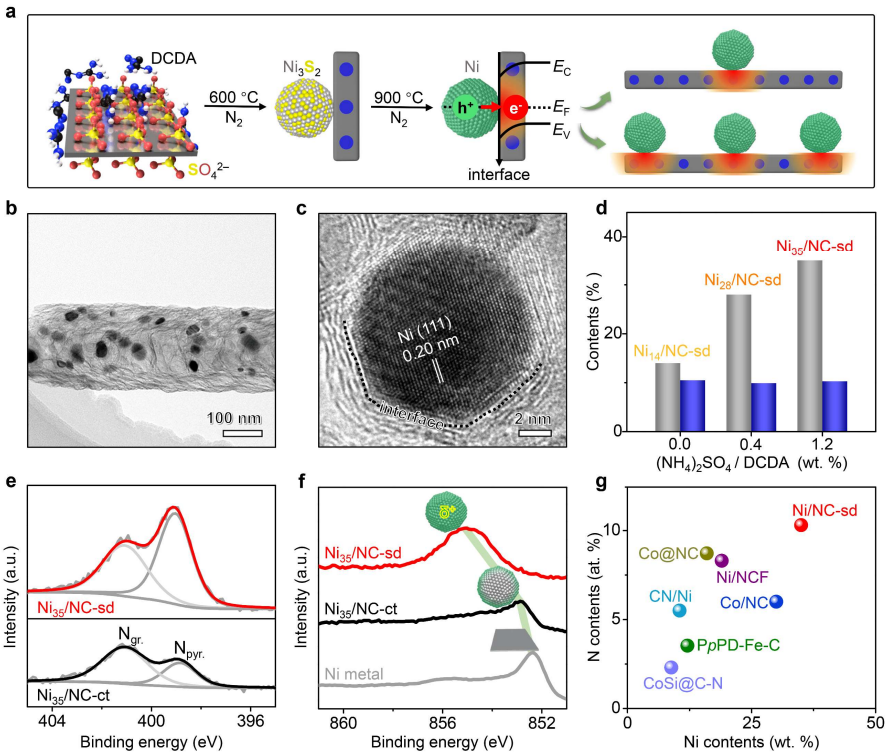

Figure 1. Fabrication and structures of Ni_x/NC-sd catalysts. (a) Synthetic process of typical Ni/NC-sd catalyst. (b) Transmission electron microscopy (TEM) image of Ni_{35}/NC-sd. (c) High-resolution TEM (HRTEM) image of Ni_{35}/NC-sd. (d) The Ni contents (wt. %, demonstrated by inductively coupled plasma (ICP-AES) analysis) and N contents (at. %, demonstrated by X-ray photoelectron spectroscopy (XPS) analysis) of Ni_x/NC-sd samples. (e) N 1s XPS spectra of Ni_{35}/NC-sd and Ni_{35}/NC-ct. (f) Ni 2p XPS spectra of Ni_{35}/NC-sd, Ni_{35}/NC-ct and Ni metal plate. (g) The metal and N contents of Ni_{35}/NC-sd and those bench-marked transition metal/NC nanocomposites in the literature.

that of Ni_x/NC-ct sample with most of pyridinic nitrogen atoms consumed (Figure 1e) by carbothermal reduction of Ni (II) species (Figure S7) even in the presence of similar dosage of dicyandiamide, reflected by the higher work function of Ni_{35}/NC-sd according to the ultroviolet photoelectron spectroscopy (UPS) results (Figure S8). The HRTEM image (Figure 1c) clearly shows the formation of a highly coupled interface of Ni metals and carbon layers.

The formation of a rectifying contact with spontaneous electron flowing at the Ni/NC interface is further confirmed by the shift of Ni 2p XPS peak of typical Ni_{35}/NC-sd of 2.7 eV to higher binding energy as to that of with bare Ni metal centered at 852.3 eV (Figure 1f). The extended X-ray absorption fine structure analysis results of typical Ni_{35}/NC-sd sample present strong Ni-Ni peak at 2.18 Å without detectable signal of any nitride/carbide/oxide component (Figure S9 and Table S3), which doubly confirm the formation of electron-deficient Ni metal nanoparticles due to the electron exchange at the interface without changing the oxidation state of Ni metal. As a control sample with the same Ni loading but less N dopant left during the carbothermal process, the Ni_{35}/NC-ct sample only exhibits a slightly positive shift of 0.6 eV (Figure 1f), again speaking for the advantage of our sulfur-diffusion method for simultaneously maintaining the strong interactions of a large amount of Ni nanoparticles with the N-rich carbon support against conventional carbothermal methods. Surprisingly, we could increase the content of Ni metal nanoparticles as high as 35 wt. % in the Ni_{35}/NC-sd sample with a nitrogen content of 10.2 at. % (Figure 1g), far surpassing the contents of the metal and N components of bench-marked transition metal/NC nanocomposites in the literature (Table S2).

Enlightened by the success in integrating high density of electron-deficient Ni nanoparticles in N-rich carbon support, we initially evaluated the performance of as-formed Ni_x/NC-sd materials as multifunctional catalysts for NO_3^- and NO_2^- reduction under ambient conditions in neutral electrolyte. The largely increased current densities in the LSV curves (Figure 2a) of the Ni_{35}/NC-sd electrocatalyst after the addition of 0.3 M $NaNO_3$ or $NaNO_2$ to the neutral Na_2SO_4 electrolyte directly indicate the electrocatalytic activity for NO_x^- reduction. The ^{1}H NMR analysis results on the reduction products only give obvious signals of ammonia (Figure 2b and Figure S10), demonstrating the high activity and selectivity to ammonia of the Ni_{35}/NC-sd electrocatalyst for reduction of both NO_3^- and NO_2^-. Blank experiments without the addition of $NaNO_3$, $NaNO_2$ or a working voltage could not generate detectable amount of ammonia (Figure S11), eliminating the possible interference of electrolyte and external environment on the quantification results. The ^{15}N isotopic labeling experiments (Figure 2b) further confirm the real role of Ni_{35}/NC-sd as an efficient electrocatalyst for selectively reducing $^{15}NO_3^-$ and $^{15}NO_2^-$ to pure $^{15}NH_3$. Remarkably, the Ni_{35}/NC-sd catalyst could offer a NH_3 yield rate of 1.2 mg h^{-1} cm^{-2} at −0.5 V versus RHE, outperforming the acid-etched Ni/NC-sd-H^+, bare nitrogen-doped carbons (NC) and Ni powder electrocatalysts by a factor of 8, 6 and 3 (Figure 2c and Figure S12), respectively. It should be noted that the Ni_{35}/NC-ct catalyst with a similar Ni loading and interfacial nanostructure could only give a NH_3 yield rate of 0.6 mg h^{-1} cm^{-2} under fixed conditions (Figure S13). More importantly, the Ni_{35}/NC-sd catalyst with more pronounced charge redistribution at the interface also gives the highest Faradaic efficiency of 99 % for NO_3^- reduction (Figure 2c) among all control samples (Figure S14), rather speaking for the key importance of the well-maintained nitrogen dopant concentrations of carbon support in our sulfur-diffusion method to boosting the interfacial synergy for NO_x^- selective reduction.

10.1002/anie.202107858

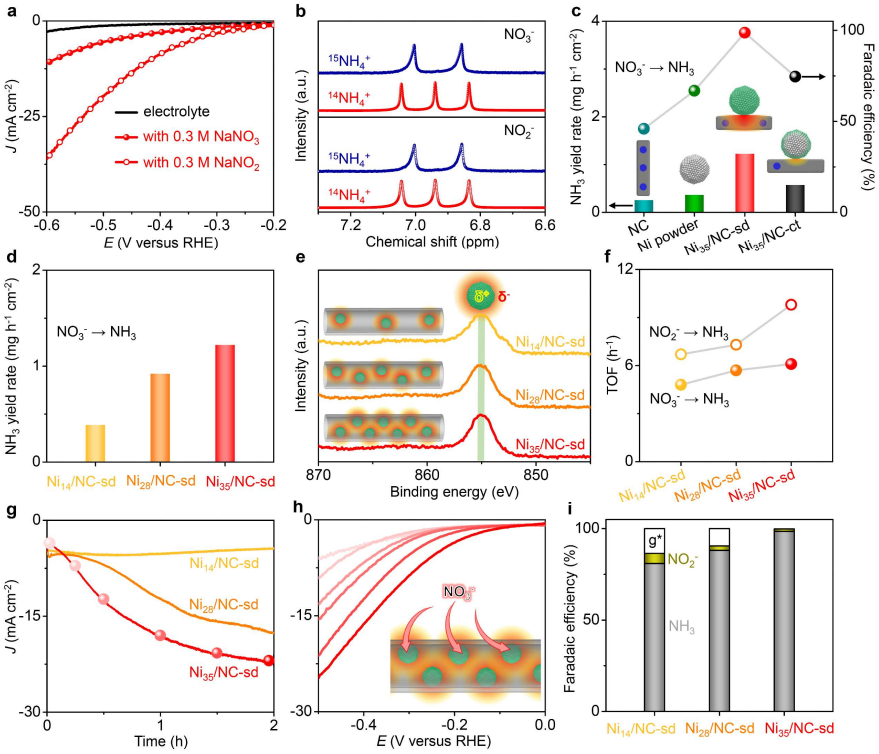

Figure 2. Electrocatalytic performance of Ni_x/NC-sd samples for NO_x^- reduction. (a) Linear sweep voltammogram (LSV) curves of Ni_{35}/NC-sd electrode in electrolyte with and without 0.3 M NO_3^- or NO_2^-. (b) ^{1}H NMR spectra of the resultant electrolyte using $^{15}NO_3^-$, $^{14}NO_3^-$, $^{15}NO_2^-$ and $^{14}NO_2^-$ as the nitrogen source. (c) NH_3 yield rates and Faradaic efficiencies of bare NC, Ni powder, Ni_{35}/NC-sd and Ni_{35}/NC-ct electrodes for NO_3^- reduction. (d) NH_3 yield rates of Ni_x/NC-sd electrodes for NO_3^- reduction. (e) Ni 2p XPS spectra of Nix/NC-sd samples. (f) The turnover frequency (TOF) values of Ni_x/NC-sd electrodes for NH_3 generation via NO_3^- and NO_2^- reduction. (g) The i-t curves of Ni_x/NC-sd electrodes for NO_3^- reduction and corresponding LSV working curves (h) of Ni_{35}/NC-sd electrode in different time periods. (i) Faradaic efficiencies of Ni_x/NC-sd electrodes for NO_3^- reduction. Standard conditions: All electrodes with the same catalyst loadings of 2.0 mg cm^{-2} were measured at -0.5 V versus RHE in 0.5 M Na_2SO_4 electrolyte with 0.3 M NO_3^- or NO_2^-.

Indeed, the change in densities of Ni/NC heterojunctions of Ni_x/NC-sd catalysts dominates the NO_x^- reduction process. It is reasonable that merging more Ni/NC active centers in one catalyst will increase the yields of ammonia accordingly as presented in Figure 2d. The electron densities of the Ni nanoparticles in all Ni_x/NC-sd samples are nearly the same without obvious shift of Ni 2p XPS peaks (Figure 2e) again due to the well-maintained nitrogen concentrations of carbon support in our sulfur-diffusion method. Even with similar electron densities and interfacial structures of Ni/NC heterojunctions, the intrinsic activities of Ni_x/NC-sd as indicated by corresponding turnover frequency (TOF) values are gradually promoted by elevating the densities of Ni/NC heterojunctions with similar trends of Ni_{35}/NC-sd > Ni_{28}/NC-sd > Ni_{14}/NC-sd for NO_3^- and NO_2^- reduction reactions (Figure 2f and Figure S15). Increasing the densities of Ni/NC heterojunctions in Ni_x/NC-sd catalysts also gives even faster increases in reduction current densities of NO_3^- (Figure 2g). With the known concentration-dependent current output for NO_3^- reduction on the Ni_{35}/NC-sd electrocatalyst (Figure S16), we could directly connect the gradually enhanced NO_3^- reduction activity (Figure 2h) and most importantly the selectivity to ammonia (Figure 2i and Figure S17) with the surface-induced in situ enrichment of NO_3^- near the electrocatalyst surface.

To further explore the surface-induced enrichment behaviour of NO_3^- anions on Ni_{35}/NC-sd catalyst, the surface charges of various Ni_x/NC-sd samples are carefully analyzed using Kelvin probe force microscopy techniques (Figure 3a).[10] With similar heights (Figure S18), the Ni_{35}/NC-sd with more Ni/NC heterojunctions integrated inside exhibits more negative the contact potential difference (ΔV) between the Si substrate and the sample (-0.148 V), which is two times of the value of Ni_{14}/NC-sd sample (Figure 3b). It is reasonable that merging more Ni/NC heterojunctions into one sample enlarges the negatively charged surface field located on the carbon support via accepting more electrons from the Ni nanoparticle-based electron donors as already demonstrated in Figure 1f and 2c.

The Schottky barrier-induced surface electric field effectively enhances the adsorption of NO_x^- anions. We use finite-element numerical method to estimate the quantitative impact of the surface electric field of negatively charged carbon support and positively charged Ni nanoparticle surface on the surface-adsorbed anion concentration.[11] As compared with the negligible effect of neutral surface (Figure S19), the charged electrode with localized electric field could largely increase the NO_x^- anions density in the Helmholtz layer of the electrical double layer adjacent to the positively charge surface with a size of 30×10 nm to mimic the electron-deficient Ni nanoparticles (Figure 3c) on the basis of the calculated number of electrons donated from Ni metal cluster to NC support by the density functional theory (DFT) calculation (Figure S20 and S21)[12], whilst the NO_x^- anions density adjacent to the negatively charged support surface is depressed accordingly. More importantly, the calculated surface adsorbed NO_x^- anions density on the mimicked Ni surface could increase from 1 to 1.63 mM just simply by introducing a slight amount of positive charges (0.03 C/m^2), theoretically demonstrating the key role of Schottky barrier-induced surface electric field in enhancing the adsorption of NO_x^- anions as already observed in previous reaction process (Figure 2e-g).

Both experimental and theoretical results demonstrate the key role of surface electric field induced by Schottky barrier in universally

10.1002/anie.202107858

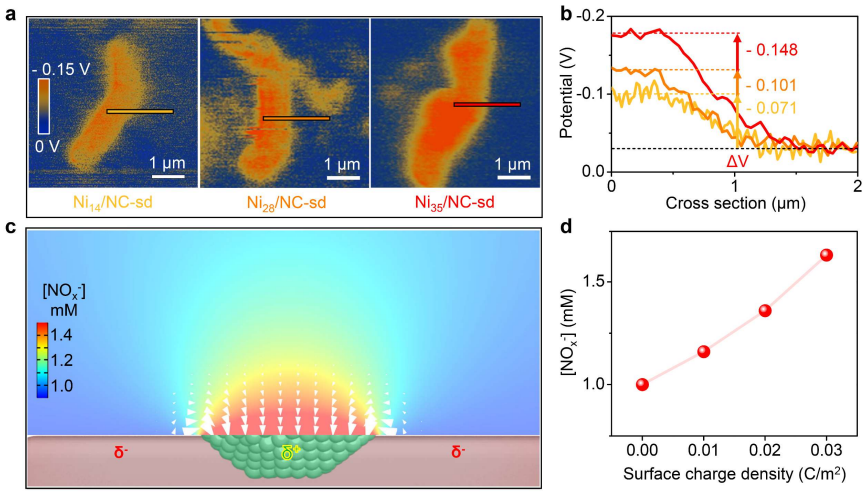

Figure 3. Effect of surface electric field of Ni_x/NC-sd samples on NO_x^- capture. (a) Surface Electric field distribution of Ni_x/NC-sd samples measured using Kelvin probe atomic force microscopy. (b) Surface potential values extracted across the lines in a. (c) The NO_x^- anions distribution on the surface of electrode, which is shown as a color map. The size and direction of each arrows represent the density and position of NO_x^- anions. (d) The NO_x^- anions density in the Helmholtz layer of the electrical double layer under different surface charge density, the Helmholtz layer is taken as the radius of hydrated NO_3^- anion (0.34 nm).[13]

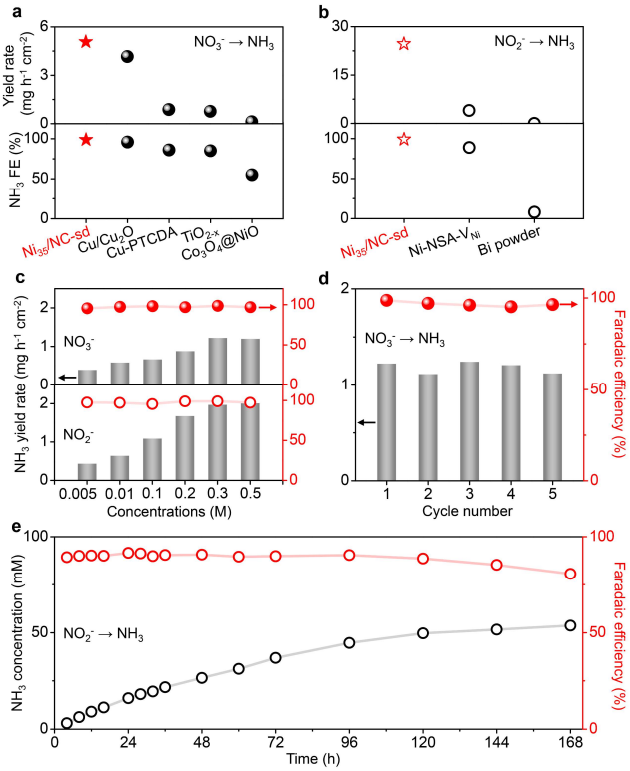

Figure 4. Activity and stability of Ni_{35}/NC-sd electrocatalyst. Electrocatalytic performance of the Ni_{35}/NC-sd electrocatalyst and state-of-the-art non-noble metal based electrocatalysts in the literature for (a) NO_3^- and (b) NO_2^- reduction to NH_3 (Table S4-S5). (c) NH_3 yield rates and Faradaic efficiencies of Ni_{35}/NC-sd electrode for NO_3^- and NO_2^- reduction in 0.5 M Na_2SO_4 electrolyte with different concentrations of NO_3^- and NO_2^-. (d) NH_3 yield rates and Faradaic efficiencies of five runs of NO_3^- reduction over a reused Ni_{35}/NC-sd electrode for two hours in 0.5 M Na_2SO_4 electrolyte with 0.3 M NO_3^-. (e) NH_3 yields and Faradaic efficiencies of Ni_{35}/NC-sd electrode for NO_2^- reduction in pure 0.3 M NO_2^- solution. Standard conditions: All electrodes with the same catalyst loadings of 2.0 mg cm^{-2} were measured at -0.5 V versus RHE.

promoting the electrocatalytic NO_x^- reduction processes. As the best-in-class catalyst in this work, the Ni_{35}/NC-sd electrocatalyst provides satisfied Faradaic efficiencies of 99 % for electrocatalytic reduction of NO_3^- (Figure 4a) and NO_2^- (Figure 4b) in neutral solution under optimized catalyst loadings (2.0 mg cm^{-2}, Figure S22) and working potentials (at -0.5 V versus RHE, Figure S23-S24). The ammonia generation yield rate on the Ni_{35}/NC-sd electrocatalyst could reach a maximum of 5.1 mg h^{-1} cm^{-2} and 25.1 mg h^{-1} cm^{-2} for electrocatalytic NO_3^- (Figure 4a) and NO_2^- (Figure 4b) reduction, respectively, far outperforming the values of state-of-the-art non-noble metal-based electrocatalysts in the literature (Figure 4a-b and Table S4-S5).

Besides very high activity, the Ni_{35}/NC-sd electrocatalyst could also provide excellent Faradaic efficiencies between 96-99 % to ammonia for the reduction of a wide range of concentrations of NO_3^- (Figure S16) or NO_2^- (Figure S25) from 5 mM to 0.5 M (Figure 4c). Surprisingly, the yield rate of ammonia on the Ni_{35}/NC-sd electrocatalyst in 5 mM NO_2^- solution (0.4 mg h^{-1} cm^{-2}) is one fifth of that in 0.5 M NO_2^- solution (2.0 mg h^{-1} cm^{-2}), indicating the ability of our catalyst surface to capture NO_2^- anions to accelerate the following reduction process. Similar trend of the enrichment phenomenon on the catalyst surface is also observed for the reduction of diluted NO_3^- solution. Moreover, such a high activity of the Ni_{35}/NC-sd electrocatalyst could be consistently reproduced during following five circles of reuses (exemplified with NO_3^- reduction in Figure 4d and Figure S26) accompanied with well-maintained nanostructures, rather speaking for the great potential of our Ni_{35}/NC-sd material as powerful and durable catalyst for electrocatalytic removal of NO_x^- anions in practical water system and ammonia production. We thus further explore the possibility of applying our electrocatalyst to NO_x^- removal, rather than the way in various electrolyte in the literature. Taking the removal of toxic NO_2^- anions as an example, we could gradually reduce pure 0.3 M $NaNO_2$ solution into ammonia (Figure 4e) with good Faradaic efficiencies (81-92 %) and give an ammonia yield of 53.7 mM within 168 h.

In summary, we have demonstrated the key role of Schottky barrier-induced surface electric field in boosting the NO_x^- reduction in water for highly efficient ammonia production. The tunable amounts of Ni nanoparticles inside nitrogen-rich carbon support on the basis of our sulfur-diffusion synthetic method afford us the ability to gradually

enhance the surface electric field for enriching and fixation of NO_x^- anions on electron-deficient Ni surface, ensuring the final Faradaic efficiency and yield rate for ammonia production. More importantly, this strategy of inducing the surface electric field by increasing the density of metal nanoparticles and thus the rectifying interfaces in various cheap and stable nanocarbons could largely widen the potential applications of durable Mott-Schottky catalysts with enhanced novel functions to a great extent in electric power storage, water purification, and even electrochemical organic synthesis.

Acknowledgements

This work was supported by the National Natural Science Foundation of China (21931005, 21720102002, and 22071146), Shanghai Science and Technology Committee (19JC1412600 and 20520711600) and the SJTU-MPI partner group. The authors thank the Shanghai Synchrotron Radiation Facility for providing beam time (BL14W1).

Key Words: Schottky barrier · surface electric field · sulfur-diffusion · NO_x^- removal · heterogeneous catalysis

[1] a) J. G. Chen, R. M. Crooks, L. C. Seefeldt, K. L. Bren, R. M. Bullock, M. Y. Darensbourg, P. L. Holland, B. Hoffman, M. J. Janik, A. K. Jones, M. G. Kanatzidis, P. King, K. M. Lancaster, S. V. Lymar, P. Pfromm, W. F. Schneider, R. R. Schrock, *Science* **2018**, 360, eaar6611; b) J. N. Galloway, J. D. Aber, J. W. Erisman, S. P. Seitzinger, R. W. Howarth, E. B. Cowling, B. J. Cosby, *BioScience* **2003**, 53, 341-356; c) J. A. Camargo, Á. Alonso, *Environ. Int.* **2006**, 32, 831-849.

[2] a) D. E. Canfield, A. N. Glazer, P. G. Falkowski, *Science* **2010**, 330, 192-196; b) V. Rosca, M. Duca, M. T. de Groot, M. T. M. Koper, *Chem. Rev.* **2009**, 109, 2209-2244; c) C. Tang, S. Z. Qiao, *Chem. Soc. Rev.* **2019**, 48, 3166-3180; d) Y. C. Zeng, C. Priest, G. F. Wang, G. Wu, *Small Methods* **2020**, 4, 2000672; e) M. Duca, M. T. M. Koper, *Energy Environ. Sci.* **2012**, 5, 9726; f) Z. H. Xue, S. N. Zhang, Y. X. Lin, H. Su, G. Y. Zhai, J. T. Han, Q. Y. Yu, X. H. Li, M. Antonietti, J. S. Chen, *J. Am. Chem. Soc.* **2019**, 141, 14976-14980; g) G. Y. Zhai, D. Xu, S. N. Zhang, Z. H. Xue, H. Su, Q. Y. Yu, H. H. Wang, X. Lin, Y. X. Lin, L. H. Sun, X. H. Li, J. S. Chen, *Adv. Funct. Mater.* **2020**, 30, 2005779.

[3] a) S. Ghafari, M. Hasan, M. K. Aroua, *Bioresour. Technol.* **2008**, 99, 3965-3974; b) P. Tavares, A. S. Pereira, J. J. G. Moura, I. Moura, *J. Inorg. Biochem.* **2006**, 100, 2087-2100; c) J. C. Fanning, *Coord. Chem. Rev.* **2000**, 199, 159-179; d) S. Samatya, N. Kabay, Ü. Yüksel, M. Arda, M. Yüksel, *React. Funct. Polym.* **2006**, 66, 1206-1214; e) C. A. Clark, C. P. Reddy, H. Xu, K. N. Heck, G. H. Luo, T. P. Senftle, M. S. Wong, *ACS Catal.* **2019**, 10, 494-509.

[4] a) Y. T. Wang, W. Zhou, R. R. Jia, Y. F. Yu, B. Zhang, *Angew. Chem. Int. Ed.* **2020**, 59, 5350-5354; b) G. F. Chen, Y. F. Yuan, H. F. Jiang, S. Y. Ren, L. X. Ding, L. Ma, T. P. Wu, J. Lu, H. H. Wang, *Nat. Energy* **2020**, 5, 605-613; c) R. R. Jia, Y. T. Wang, C. H. Wang, Y. F. Ling, Y. F. Yu, B. Zhang, *ACS Catal.* **2020**, 10, 3533-3540; d) Y. T. Wang, C. B. Liu, B. Zhang, Y. F. Yu, *Science China Materials* **2020**, 63, 2530-2538; e) J. X. Liu, T. T. Cheng, L. Q. Jiang, A. G. Kong, Y. K. Shan, *ACS Appl. Mater. Inter.* **2020**, 12, 33186-33195; f) J. Y. Zhu, Q. Xue, Y. Y. Xue, Y. Ding, F. M. Li, P. J. Jin, P. Chen, Y. Chen, *ACS Appl. Mater. Inter.* **2020**, 12, 14064-14070; g) P. H. van Langevelde, I. Katsounaros, M. T. M. Koper, *Joule* **2021**, 5, 290-294.

[5] a) E. Pérez-Gallent, M. C. Figueiredo, I. Katsounaros, M. T. M. Koper, *Electrochim. Acta* **2017**, 227, 77-84; b) X. B. Fu, X. G. Zhao, X. B. Hu, K. He, Y. N. Yu, T. Li, Q. Tu, X. Qian, Q. Yue, M. R. Wasielewski, Y. J. Kang, *Appl. Mater. Today* **2020**, 19, 100620; c) J. Li, G. M. Zhan, J. H. Yang, F. J. Quan, C. L. Mao, Y. Liu, B. Wang, F. C. Lei, L. J. Li, A. W. M. Chan, L. P. Xu, Y. B. Shi, Y. Du, W. C. Hao, P. K. Wong, J. F. Wang, S. X. Dou, L. Z. Zhang, J. C. Yu, *J. Am. Chem. Soc.* **2020**, 142, 7036-7046; d) Y. H. Wang, A. Xu, Z. Y. Wang, L. S. Huang, J. Li, F. W. Li, J. Wicks, M. C. Luo, D. H. Nam, C. S. Tan, Y. Ding, J. W. Wu, Y. W. Lum, C. T. Dinh, D. Sinton, G. F. Zheng, E. H. Sargent, *J. Am. Chem. Soc.* **2020**, 142, 5702-5708.

[6] a) C. H. Wang, W. Zhou, Z. J. Sun, Y. T. Wang, B. Zhang, Y. F. Yu, *J. Mater. Chem. A* **2021**, 9, 239-243; b) D. P. He, Y. M. Li, H. Ooka, Y. K. Go, F. M. Jin, S. H. Kim, R, Nakamura, *J. Am. Chem. Soc.* **2018**, 140, 2012-2015.

[7] a) H. Su, L. H. Sun, Z. H. Xue, P. Gao, S. N. Zhang, G. Y. Zhai, Y. M. Zhang, Y. X. Lin, X. H. Li, J. S. Chen, *Chem. Commun.* **2019**, 55, 11394-11397; b) P. F. Zhang, L. Wang, S. Z. Yang, J. A. Schott, X. F. Liu, S. M. Mahurin, C. L. Huang, Y. Zhang, P. F. Fulvio, M. F. Chisholm, S. Dai, *Nat. Commun.* **2017**, 8, 15020; c) J. S. Meng, C. J. Niu, L. H. Xu, J. T. Li, X. Liu, X. P. Wang, Y. Z. Wu, X. M. Xu, W. Y. Chen, Q. Li, Z. Z. Zhu, D. Y. Zhao, L. Q. Mai, *J. Am. Chem. Soc.* **2017**, 139, 8212-8221.

[8] a) X. H. Li, M. Antonietti, *Chem. Soc. Rev.* **2013**, 42, 6593-6604; b) Y. X. Lin, S. N. Zhang, Z. H. Xue, J. J. Zhang, H. Su, T. J. Zhao, G. Y. Zhai, X. H. Li, M. Antonietti, J. S. Chen, *Nat. Commun.* **2019**, 10, 4380; c) H. Su, K. X. Zhang, B. Zhang, H. H. Wang, Q. Y. Yu, X. H. Li, M. Antonietti, J. S. Chen, *J. Am. Chem. Soc.* **2017**, 139, 811-818.

[9] a) C. Buchmaier, M. Glänzer, A. Torvisco, P. Poelt, K. Wewerka, B. Kunert, K. Gatterer, G. Trimmel, T. Rath, *J. Mater. Sci.* **2017**, 52, 10898-10914; b) G. Kullerud, R. A. Yund, *J. Petrol.* **1962**, 3, 126-175.

[10] a) R. T. Chen, S. Pang, H. Y. An, J. Zhu, S. Ye, Y. Y. Gao, F. T. Fan, C. Li, *Nat. Energy* **2018**, 3, 655-663; b) X. J. Chen, Y. Xu, X. G. Ma, Y. F. Zhu, *Natl. Sci. Rev.* **2020**, 7, 652-659; c) Y. Guo, W. X. Shi, Y. F. Zhu, *EcoMat* **2019,** 1, e12007.

[11] a) M. Liu, Y. J. Pang, B. Zhang, P. D. Luna, O. Voznyy, J. X. Xu, X. L. Zheng, C. T. Dinh, F. J. Fan, C. H. Cao, F. P. G. de Arquer, T. S. Safaei, A. Mepham, A. Klinkova, E. Kumacheva, T. Filleter, D. Sinton, S. O. Kelley, E. H. Sargent, *Nature* **2016**, 537, 382-386; b) P. Liu, B. Chen, C. W. Liang, W. T. Yao, Y. Z. Cui, S. Y. Hu, P. C. Zou, H. Zhang, H. J. Fan, C. Yang, *Adv. Mater.* **2021**, 33, 2007377.

[12] Z. H. Xue, J. T. Han, W. J. Feng, Q. Y. Yu, X. H. Li, M. Antonietti, J. S. Chen, *Angew. Chem. Int. Ed.* **2018**, 57, 2697-2701.

[13] V. G. Volkov, S. Paula, D. W. Deamer, *Bioelectrochem. and Bioenerg.* **1997**, 42, 153-160.

10.1002/anie.202107858

Entry for the Table of Contents

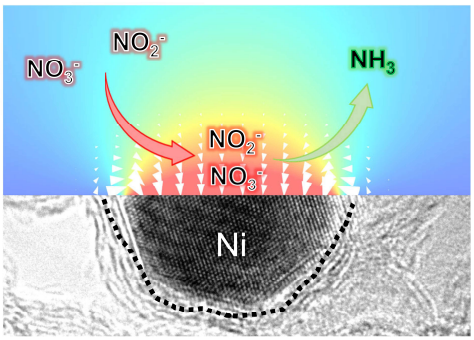

We initially discovered the conceptual application of the tunable surface electric field induced by Schottky barrier boosts the reduction of NO_x^- in water for highly efficient ammonia production. The tunable amounts of Ni nanoparticles inside nitrogen-rich carbon support on the basis of our sulfur-diffusion synthetic method could afford us the ability to gradually enhance the surface electric field for enriching and fixation of NO_x^- anions on electron-deficient Ni surface, rendering high Faradaic efficiency of 99 % for ammonia production from both electrocatalytic NO_3^- and NO_2^- reduction.